Computational analysis on the transient movement of helices in sensory rhodopsin II

Authors; Y. Sato[†], M. Hata, S. Neya, T. Hoshino[*]

Affiliations; Graduate School of Pharmaceutical Sciences, Chiba University

Address Chiba 263-8522, Japan

[†]**present address** Japan Biological Information Research Center (JBIRC) Time24 Bldg. 10F 2-45 Aomi, Koto-ku, Tokyo 135-0064 Japan

[*]**corresponding author** Tyuji Hoshino,

Postal address Graduate School of Pharmaceutical Sciences, Chiba University
Chiba 263-8522, Japan

Tel number +81-43-290-2926

Fax number +81-43-290-2925

e-mail address hoshi@p.chiba-u.ac.jp

running title Transient movement of helices in SR II

Total number of pages 21**, supplementary pages** 0**, Tables** 3**, Figures** 10

Word processor MicroSoft Word

[Abstract]

MD simulation of sensory rhodopsin II was executed for three intermediates (ground state,K-state,M-state) appearing in its photocycle. We observed a large displacement of the cytoplasmic side of helixF only in M-state among the three intermediates. This displacement was transmitted to TM2, and the cytoplasmic side of TM2 rotated clockwisely. These transient movements are in agreement with the results of EPR experiment. That is, the early stage of signal transduction in sRII – HtrII complex was successfully reproduced by the *in silico* MD simulation. By analyzing the structure of sRII – HtrII complex, the following findings about the photocycle of sRII were obtained. (1)The hydrogen bonds between helixF and other helices determine the direction of the movement of helixF. (2) Three amino acids (Arg162,Thr189,Tyr199) are essential for the sRII-HtrII binding and contribute to the motion transfer from sRII to HtrII. (3)After the isomerization of retinal, a major conformational change of retinal was caused by proton transfer from Schiff base to Asp75, which in turn triggers the steric collision of retinal with Trp171. This is the main reason for the movement of the cytoplasmic side of helixF.

[Keywords]

Sensory rhodopsin II, molecular dynamics simulation, signal transduction, transducer, movement of helixF

[Abbreviations and symbols]

sRII : Sensory Rhodopsin II

HtrII : transducer molecule

TM : transmembrane

BR : BacterioRhodopsin

MD : Molecular Dynamics

RMSD : Root Mean Square Deviation

VDW : van der Waals

[Introduction]

Sensory rhodopsin II (sRII) is a membrane protein that functions as a sensor for phototactic avoidance of blue-green light in the cell membrane of *Natronobacterium pharaonis* (Takahashi et al., 1985, 1990). The transmission of photo-signal from the photoreceptor sRII to the following cytoplasmic signal cascade is achieved by a transducer molecule that binds tightly and specifically to its cognate receptor (Zhang et al., 1999). This transducer molecule consists of two transmembrane helices (TM1 and TM2). The function of sRII is activated through a cyclic process initiated by the absorption of a photon. The photocycle is characterized by a series of intermediates $sRII_{498}$,K_{540},L_{488},M_{390},$O_{560,}$ where the subscripts denote the wavelengths of the respective absorption maxima (Kamo et al,2001).

The photocycle of sRII is effectuated by a retinal chromophore which is bound to the Lys205 residue through a Schiff base linkage. Retinal undergoes an electronic excitation and shows photochemical transformation. In $sRII_{498}$, retinal is in the all-trans configuration. A photon triggers an isomerization of retinal and leads to the transition $sRII_{498}\rightarrow K_{540}$.The intermediate K_{540} which contains a strained 13-cis configuration of retinal thermally decays to L_{488} (Kandori et al. 2001).

During the $L_{488}\rightarrow M_{390}$ transition, the proton bound to retinal's Schiff base is transferred to Asp75 (Sasaki et al., 1999, Furutani et al. 2002). It was clarified by the electron paramagnetic resonance spectroscopy experiment that the outward movement of cytoplasmic side of helixF occurs before M-state (Wegener et al., 2000). The movement of helixF triggers a rotation of its transducer (TM2) (Klare et al., 2004), and its transformation is converted to the cytoplasmic cellular signal. Recently, the X-ray structure of the complex of *Natronobacterium pharaonis* sRII with the receptor-binding domain of HtrII was obtained at 1.93 Å resolution (Gordeliy et al., 2002), and it provided an atomic picture of the first step of the signal transduction.

Molecular dynamics simulation can observe the dynamic fluctuation of the protein structure with a fs time scale and in an atomic level. This is an advantage of computer simulation from other experimental methods. In our previous *ab initio* computational study about BR (Murata et al., 2003, 2002, 2000) which is same bacterial retinal protein, we proposed the importance of internal water chain for the proton pump activity. These internal water molecules are often difficult to be detected by experimental methods such as crystallographic study. The validity of this proposal has been proved in some

different groups' studies (Schobert et al., 2003; Lee, 2004). Similarly, the molecular dynamics simulation on the sRII-HtrII complex is expected to clarify the mechanism of signal transduction more clearly. In this study, we performed molecular dynamics simulations of the three intermediates (ground state, K-state, M-state) in sRII's photo-cycle, and observed the motion of atoms when sRII transmits the signal to the transducer (HtrII).

[Results and Discussion]

We simulated *Natronobacterium pharaonis* sRII in the three different intermediates. In the simulation, the atoms constituting the lipid bilayer and water molecules were included along with the sRII and HtrII protein. Fig.1 shows the simulation model for this sRII-HtrII, lipid-bilayer, and water molecule system. More details are provided in Materials and Methods. In the following, we report several findings about the signal transduction in sRII – HtrII complex deduced from the present computer simulations.

RMSD, thickness of lipid bilayer and retinal surroundings in three intermediates

First of all, root mean square deviation (RMSD) from the energy minimized structure was respectively examined in three intermediates simulations. The RMSD value was extracted only from the backbone atoms of sRII – HtrII complex to neglect the minor fluctuation of side chains. In the respective simulation, RMSD value rapidly changed in the heating calculation for first 60ps and almost kept constant during the following 500ps simulation at 310K. The average RMSD value during the M-state simulation (0-500ps) is 1.7Å, and this is the largest among the three intermediates. The next one is of the K-state (1.5Å), and the smallest is of the ground state simulation (0.8Å).

Then, the change of the thickness of lipid bilayer along the total of 560ps simulation was examined (Fig2). The thickness is defined as the distance between the average z-position of oxygen atoms in the hydroxyl group of the glycerol located at the cytoplasmic side and the average z-position of oxygen atoms at the extracellular side, each of those oxygen atoms makes an ester bond to the fatty acid chains in lipid molecules(PGP-Me). This value gradually decreased with the progress of simulation mainly in the first 60ps heating simulation and approached a constant value. The averaged thickness value for the last 200ps (300ps ~ 500ps) of the simulation is 31.61Å and consistent with the experimentally measured thickness

by electron diffraction of *Harobacterium salinarium* (Mitsuoka et al., 1999). This indicates that the present simulation for lipid- protein model system successfully reproduces the physiological condition.

We also analyzed the change of the interaction of the retinal with surrounding amino acid residues following the retinal photoisomerization. Fig 3 shows the change of the distances between Schiff base and two amino acid side chains as a function of simulation time. One notable binding factor is the hydrogen bond between Schiff base and hydroxyl oxygen atom of Thr79 (Fig 3(a)), and the other is the hydrogen bond between Schiff base and calboxyl oxygen atom of Asp201 (Fig 3(b)). Asp201 has two equivalent calboxyl oxygen atoms in its side chain, but we focus only the nearer one to the Schiff base. The distance between Schiff base and hydroxyl oxygen of Thr79 was close in K-state and ground state, but it was more distant in M-state. On the other hand, the distance between Schiff base and calboxyl oxygen atom of Asp201 was close in K-state compared to other two intermediates. In only K-state, the Schiff base made the hydrogen bonds with hydroxyl oxygen atom of Thr79 as well as calboxyl oxygen atom of Asp201, and these hydrogen bonds disappeared in M-state. According to the changes in these hydrogen bond interactions and the retinal conformation, we summarize the pattern of chromophore-protein interaction in the three intermediates as follows. In ground state, the retinal has an all-trans conformation, and the Schiff base proton faces to the direction of the extracellular region. The retinal stably interacts with hydroxyl oxygen atom of Thr79 in extracellular region. After retinal photoisomerization, retinal has the strained 13-cis conformation, and the Shiff base proton turns to the reverse direction, i.e., the opposite of the extracellular region. In spite of this conformational change, the Schiff base proton still interacts with two residues in the extracellular region. This Shiff base protonation state is fairy instable, and would result in the proton release to the Asp75 in the extracellular region. In M-state, the interaction with extracellular region disappears due to the Schiff base proton release to the Asp75, and the instable chromophore-protein interaction is cancelled and the constraint retinal structure recovers to the stable form.

Inter-helical Hydrogen bonds from helixF

Inter-helical hydrogen bonding was surveyed between helixF and the other helices of sRII, using the data of the ground state simulation. The criteria for keeping a hydrogen bond with the donor – H – acceptor formation is the following two :

(1) within 4Å for the distance between donor and acceptor atoms (2)within 60 degree for the H – donor – acceptor angle. Table1 shows inter helical hydrogen bonds that meet the criteria for more than 30% of time in the 500ps simulation. Totally 12 hydrogen bonds were detected between helixF and other helices. In nine cases of them, the amino acid residues of helixF are in the donor character, and in three cases the amino acids of helixF are acceptor. 6 hydrogen bonds are located in the cytoplasmic half side, and the remaining 6 bonds were in the extracellular half side. The total number of the amino acid residues participating in these hydrogen bonds is 13, and 8 amino acid residues of them are conserved in the corresponding sequence of BR (*Halobacterium salinarium*). If the carbonyl group of main chain is also taken into account for hydrogen bonds, almost all the amino acid residues participating in the inter-helical hydrogen bonds are conserved in BR. This indicates that these hydrogen bonds are essential for both BR and sRII. The significant common features between them are the presence of seven helices and the experimentally observed motion of the cytoplasmic half side of helixF (Wegener et al., 2000). Furthermore, all 6 hydrogen bonds appearing in the cytoplasmic half side are between helixF and helixE. On the other hand, the counterpart of the hydrogen bond from helixF are various (helix C,D,E,G) in the extracellular half side.(Fig.4) That is , the extracellular side of helixF have a strong interaction with other 6 helices while the cytoplasmic side is connected only to the one direction. This enables the movement of the cytoplasmic side of helixF perpendicular to the direction of helixE.

The movement of helixF

In order to clarify the mechanism for the movement of helixF, the dynamics of three intermediates (ground state, K-state, M-state) were compared from the simulation data. First, we measured the fluctuation of the distance between the center of whole protein (sRII) and the center of the cytoplasmic half side of helixF that consisted of 13 residues (res 158-170). The distances are presented in Fig.5 along the simulation time.

The distance in M-state is the largest among the three simulations, and the fluctuation is also large in M-state. This means that the cytoplasmic half side of helixF moves to the direction away from the center of sRII when sRII is in M-state. The distance in K-state is larger than that in the ground state, but the deviation from the ground state gradually became small as

the progress of the simulation. Fig.6 shows the superimposed view of the average structures for the last 50ps in the ground-state and M-state simulations. It is confirmed from this figure that the cytoplasmic half side of helixF indeed moved to the outward of the protein, and the cytoplasmic side of TM2 also moved in accordance with this movement. This movement is consistent with the result obtained by EPR experiment by Wegener et al. (Wegener et al., 2000).

In order to clarify the driving force of this movement, we measured the van der Waals(VDW) interaction energy between retinal and each amino acid residues of sRII both in the ground state and M-state simulations (Fig7-(a)). There appear seven peaks in the energy, that is, the interacting residues are divided into seven groups. These groups match to the seven helices of sRII, and helixC and helixF especially have a strong interaction with retinal. Alignment of the amino acid sequence of 16 bacterial retinal proteins also reveals a high degree of sequence conservation in helixC and helixF.(Fig7-(b)). Hence, these helices would mainly contribute to the retinal binding to the sRII or have a significant influence on the retinal structural change. Then, the energy difference between the ground state and M-state is shown in Fig7-(c). This clearly indicates that the interaction between retinal and Trp171 dramatically changed and became less stable in M-state than the ground state. We speculate that the isomerization of retinal results in this energetic instability and the recovery of this instability cause the movement of helixF.

The large movement of helixF in M-state, however, can not be explained only from the isomerization of retinal because K-state also has a 13-cis retinal structure. Hence, we compared the structure of M-state with K-state to examine the factor to enhance the retinal – Trp171 interaction other than the isomerization of retinal. The major difference between K-state and M-state is the protonation state. In the L→M conversion, the proton bound to the Schiff base transfers to the Asp75 (Sasaki et al., 2000) and the charging state of the Schiff base is converted from the positive to the neutral. Fig.8 shows the structures around the retinal both in K-state and in M-state, in which two structures are superimposed in respect to the backbone atoms of whole protein (sRII) and each structure is the average of last 50ps of the simulation. In K-state, the retinal is pulled to the direction of Thr79, because there appears a hydrogen bond connection between the Schiff base and Thr79 due to the positive charge at the Schiff base. Asp75 further supports the approach of Thr79 to the retinal by making hydrogen bond network through Schiff base – Thr79 – Asp75, because Asp75 is negatively charged in K-state. It should be

emphasized that the retinal has a strained structure in K-state. On the other hand, the retinal is released away from Thr79 in M-state, because the hydrogen bond connection with Thr79 is canceled due to the neutral charge at the Schiff base. Since Asp75 also becomes neutral, the hydrogen bond network through Schiff base – Thr79 – Asp75 disappears in M-state. The distance between the nitrogen atom of Schiff base and the hydroxyl oxygen atom of Thr79 during the last 50ps of simulation was 3.25Å in K-state and 3.39Å in M-state. This release of retinal from Thr79 causes the positional shift of retinal, which induces the steric collision of the retinal with Trp171. This collision would result in the movement of helixF in M-state.

Spudich et al reported that the D73N mutation of *Halobacterium salinarum* sRII causes the constitutive signaling in its unphotostimulated state (Spudich et al., 1997). Asp73 in *Halobacterium salinarum* sRII corresponds to Asp75 in *Natronobacterium pharaonis* sRII, and both aspartic acids may have the same role. From our structural investigation, it is clarified that this hydrogen bond network (Schiff base →Thr79 →Asp75) controls the conformation of retinal and consequently regulates the movement of helixF. The residues participating in this extracellular hydrogen bond network from Schiff base and interacting with retinal are highly conserved among retinal proteins of various species. It was reported that the outward movement of helixF also occurred in BR (Koch et al., 1991; Subramaniam, 1993). From these two facts, it is speculated that the movement of helixF is seen in other retinal proteins, and the mechanism is common among them, although each of these retinal proteins has the respective different function. Further, we speculate that sRII's function of signal transduction is induced by the ability of binding to the cognate transducer (HtrII), and BR does not have the binding ability to HtrII.

Signal transmission to HtrII

In order to investigate how the signal transmits to the receptor (HtrII), we executed additional 1.5ns MD simulation in M-state because a large movement of helixF had been observed. Accordingly totally 2ns MD simulation was performed for the M-state and the structural change of the transducer (HtrII) was examined in detail. Fig9(a) shows the conformational change of TM2 and the rotational angle of three amino acid residues (Ala79,Ala80,Thr81) in the course of

MD simulation. For determining the axis of TM2, we separated the amino acid residues in TM2 into two parts: extracellular (Residue 54-67) and cytoplasmic areas (Residue 68-82), and calculated the center point of each area. We defined the axis of TM2 as a vector connecting these two points, and calculated rotational angle of three amino acid residues from the initial structure. The cytoplasmic side of TM2 started to rotate clockwise at 1ns, followed by the appearance of a maximum rotational displacement at 1.8ns. This rotational movement of TM2 is consistent with the movement detected by the electron paramagnetic resonance experiment (Wegener et al., 2001). The degree of rotational movement is shown in Fig9(b). Three amino acid residues (Ala79,Ala80,Thr81) are located on midst of the cytoplasmic side of TM2. The movements of the side chain of these three amino residues are in the range of 2~3Å, and the average value of the rotational angle of three amino acid residues is 24.8 degree. The motion observed by EPR experiment (Wegener et al., 2001) was also in the same range. In our simulation, the rotational movement was observed in the time scale of 1ns, which suggests that the signal transduction to HtrII occurs in a considerably short time. In this study, the first signal transduction step has been successfully reproduced *in silico*. It is, however, still unclear how this TM2 transition is converted into a cellular signal. We are planning to observe this cellular signal by executing MD simulation with a larger model system including the cytoplasmic inner side of protein in future.

The recognition of HtrII by sRII

It is of great interest to clarify the reason why sRII specifically recognizes HtrII. In order to investigate the binding mechanism, we firstly examined hydrogen bonds between HtrII and sRII using the data of the ground state simulation (Table 2). The criteria for the hydrogen bond are the same as described in the measurement of the inter-helical hydrogen bond from helixF. Totally 8 hydrogen bonds were detected between HtrII and sRII. All of the amino acid residues participating in these hydrogen bonds are not conserved in the corresponding sequence of BR(*Halobacterium salinarium*). This is a marked difference from the inter-helical hydrogen bonds around helixF. BR can not bind to the HtrII, that is, the amino acid residues (Arg162,Thr189,Thr191,Tyr199) in Table2 are important for the binding of HtrII.

Secondly, we measured the interaction energy (VDW and Coulomb interaction) between HtrII and each amino acid

residues of helixF and helixG using the MM_GBSA method (Kollmann et al., 2000) (Fig 10-(a)). It is found from this measurement that five amino acid residues (R152,K157,R162,R164,Y199) have strong interaction with HtrII. The interaction energy was modified by including solvent effect energy term in addition to VDW and coulomb terms (Fig10-(b)). The amino acid residue that has the largest interaction energy with HtrII is Tyr199, and the major factor for the interaction between Tyr199 and HtrII is not the hydrophilic but the hydrophobic interaction term. This result is consistent with the result of isothermal titration calorimetry experiment (Hippler-Mreyen et al., 2003) that reported the essential role of aromatic side-chains of Tyr199 for proper binding of HtrII and sRII. Furthermore, the hydrogen bonding of Tyr199 with Asn74 of the transducer was detected in the X-ray structure (Gordeliy et al., 2002). Sudo et al (Sudo et al., 2003) reported that this Tyr199-Asn74 hydrogen bonding might not be the only cause for the sRII-HtrII binding. In our present study, the hydrogen bonding of Tyr199 with the main chain of Phe28 of transducer was observed, and this hydrogen bonding was more stable than that with Asn74. That is, Tyr199 assists the hydrophilic interaction between sRII and HtrII in addition to the significant contribution in hydrophobic interaction. This would be the reason why the interaction between Tyr199 and Phe28 of transducer is essential for the sRII – HtrII binding, as reported by Hippler-Mreyen et al. (Hippler-Mreyen et al., 2003)

Thirdly, we calculated the change of binding affinity between HtrII and sRII using MM_GBSA method, when the amino acid residues that had not been conserved in the sequence of BR in helixF and helixG were mutated to the corresponding residues of BR. Table3 shows the change of binding affinity for 9 mutations. This measurement clearly demonstrates that three amino acid residues are important for the binding. One is Arg162 that has a positive charge. When Arg162 is mutated to Val, the affinity change from the wild type is 3.99kcal/mol. This means that the substitution of Arg162 for Val decreases the binding affinity between HtrII and sRII. Several positively charged residues are distributed at the cytoplasmic end of helix F. These charged residues are not present in BR (Royant et al., 2001). Further, these positively charged residues interact with the negatively charged cytoplasmic domain of TM2 helix of HtrII, the sequence of which is conserved among various species (Seidai et al., 1995). These results suggest that Arg162 mainly contributes to the remarkable stability of the sRII-HtrII complex and the stability is due to the electrostatic interaction. In addition to this residue, Thr189 and Tyr199

show prominent affinity changes by the mutation of T189P and/or Y199V, and these two residues are also essential for the recognition of HtrII by sRII. These two amino acid residues are expected to be also important for sRI-HtrI binding in *Halobacterium halobium* sRI which binds only its cognate transducer HtrI, Our sequence analysis shows a sound similarity in binding due to Thr189 between sRII-HtrII and sRI-HtrI systems, whereas a keen contrast is seen for Tyr199. As for Thr189, this amino acid residue is conserved in the corresponding position in *Halobacterium halobium* sRI. The residues at the corresponding positions of proton acceptor Glu43 and Ser62 in *Natronobacterium pharaonis* HtrII are Asp and Asn in *Halobacterium halobium* HtrI, respectively. Both amino acid residues of Asp and Asn can act as proton acceptor from Thr like Glu43 and Ser62 in *Natronobacterium pharaonis* HtrII. We assume that the hydrogen bonds related to Thr189 in sRII-HtrII system are conserved in sRI-HtrI system. On the other hand, as for Tyr199, the residue at the corresponding position of this residue in *Halobacterium halobium* sRI is Phe. Phe has no hydroxyl side chain and can not act as hydrogen bond donor. In sRII-HtrII system, Tyr199 has three hydrogen bonds with HtrII, and the counterpart residues in HtrII are Phe28, Thr33 and Asn74 (in Table2). The residues at the corresponding positions of these residues in *Halobacterium halobium* HtrI are Ala, Leu and Ala, respectively. All these three residues have no side chains that can act as proton acceptor. Because the hydrophobic interaction also shows a large contribution for Tyr199 relating interactions in sRII-HtrII system, the hydrophobic interaction may be much emphasized in sRI-HtrI system. This is a prominent difference in binding pattern between sRII-HtrII and sRI-HtrI system. Further experimental and computational studies are needed from the viewpoint of molecular recognition.

[Materials and Methods]

Construction of the initial structure of the sRII – HtrII complex

For the ground state simulation, the initial structure was constructed based on the X-ray crystal structure (PDB code: 1H2S) (Gordeliy et al.,2002). For the K-state simulation, the crystal structure (PDB code: 1GUE) (Edman et al., 2002) was used , but this PDB code did not contain HtrII part. In order to construct the sRII – HtrII complex in K-state, the sRII structure in 1GUE was superimposed on the sRII – HtrII complex of the ground state using modeling software InsightII,

and sRII part was substituted for the complex. No crystal structure was obtained for the sRII – HtrII complex in M-state. Hence, the initial structure of M-state was constructed by changing the protonation state of the initial structure of K-state. In K-state structure, Asp75 is unprotonated and Schiff base is protonated. On the other hand, Asp75 is protonated and Schiff base is unprotonated in M-state structure.

Construction of computational models for the protein – lipid bilayer – water solvent system

In order to reproduce the environmental condition for the membrane protein, the model structure of a lipid bilayer was constructed. For the component of lipid bilayer, we selected phosphatidylglycerophosphate monomethyl ester (PGP-Me) that is a main component of purple membrane (PM) (Kates et al., 1993). This lipid is considered to be essential for the photo-cycle expression of the other retinal protein in *Halobacterium salinarium*, because the photo-cycle activity of retinal protein decrease without PGP-Me (Joshi et al., 1998). First, a piece of the lipid bilayer consisting of 160 PGP-Me molecules was constructed. Second, 56 PGP-Me molecules at the center area of the lipid bilayer were removed for the sake of making the cavity in which sRII-HtrII complex was placed. Third, sRII-HtrII complex was inserted into the cavity using modeling software (InsightII). Totally, 104 lipid molecules were arranged around the sRII – HtrII complex. Finally, 9973 water molecules were generated at the upper and lower sides of the sRII-HtrII-lipid bilayer complex up to 7Å from the edge of lipid molecules(Fig1)

Computational details

The simulations and analyses described in this paper were carried out using the AMBER program package (Case et al., 2002) together with the Amber parm99 force field (Wang et al., 2000) except for retinal. Atomic charges and stable conformation of the retinal Schiff base were deduced from *ab initio* quantum chemical calculations, where density functional theory(DFT) (Becke, 1993; Lee et al., 1988) were applied on a whole retinal Schiff base structure using GAUSSIAN98 (Frisch et al., 1998). The hybrid Becke3LYP method and 6-31G** basis set were used for the DFT calculations. The charges were computed by the RESP method (Cieplak et al., 1995). In both unprotonated and protonated

states, the same force field was assigned for retinal by using antechamber module in AMBER program package, except for the force parameter for C15-N torsion. The torsional potential was set to 28.76kcal/mol for the protonated state, and 30.0 for the unprotonated (Tajkhorshid et al., 2000). An integration time step of the simulation was chosen to be 1fs. A cut-off distance of 10Å for non-bonded interactions and a dielectric constant of ε=1 were employed. A periodic boundary condition was applied, and the pressure was kept constant for the whole system.

Minimization, Equilibration and Simulation data acquisition

First, potential energy minimizations were performed on each intermediate starting from the respective initial structure. The total step of the minimization is 10000, the first 3000 steps were executed by the steepest decent method and the last 7000 steps were by the conjugated gradient method. Next, MD simulations were performed from the respective energy minimized structure. The whole systems were gradually increased by heating up to 310K for 60ps and then kept at 310K for the next 500ps. The trajectories at 310K for 500ps were considered to be the most probable structure under the physiological conditions and were collected for analysis.

The figure of the structure in this paper was drawn by molecular visualizing software RasMol (Sayle et al., 1995) and VMD (Humphrey et al., 1996).

Alignments and calculation of the degree of sequence conservation

Amino acid sequences of bacterial retinal proteins in different species were retrieved from DB (GENES,SwissProt,TrEMBL,TrEMBL_new,PIR,PRF,PDBSTR) using BLASTP2.2.6 (Altschul et al., 1997). We used the *Natronobacterium pharaonis* sRII sequence as a query, and selected total 16 bacterial retinal proteins whose homological score is over 70. Classification of the 16 bacterial retinal proteins is as follows; BR-6,HR-4,sRI-2,sRII-4. ClustalW (Thompson et al., 1994) was used for the multiple alignments. From the data of multiple alignment, the amino acid residues of *Natronobacterium pharaonis* sRII were examined in terms of the conservativeness in sequence among 16 bacterial retinal proteins.

[Acknowledgement]

We thank Prof. Naoki Kamo at Hokkaido University for reading the manuscript and giving many important suggestions. The calculations were carried out by the DRIA system at Graduate School of Pharmaceutical Sciences, Chiba University, and at Institute of Media and Information Technology, Chiba University. This work was partly supported by a Grant-in-Aid for Center Of Excellence (COE) research from the Ministry of Education, Science, Sport, and Culture, Japan.

[References]

Altschul, Stephen, F., Madden, T.L., Schaffer, A.A., Zhang, J., Zhang, Z., Miller, W. and Lipman, D.J. 1997. Gapped BLAST and PSI-BLAST: a new generation of protein database search programs *Nucleic Acids Res.* **25**:3389-3402

Becke, A. D. 1993. Density-functional thermochemistry. III. The role of exact exchange. *J. Chem. Phys.* **98**:5648-5652.

Case, D.A., Pearlman, D.A., Caldwell, J.W., Cheatham III, T.E., Wang, J., Ross, W.S., Simmerling, C.L., Darden, T.A., Merz, K.M., Standon, R.V., Cheng, A.L., Vincent, J.J., Crowley, M., Tsui, V., Gohlke, H., Radmer, R.J., Duan, Y., Pitera, J., Massova, I., Seibel, G.L., Singh, U.C., Weiner, P.K. and Kollmann, P.A., 2002. AMBER7

Cieplak, P., Cornell, W.D., Bayly, C. & Kollman, P.A., 1995. Application to the multimolecule and multiconformational RESP methodology to biopolymers: Charge derivation for DNA, RNA and proteins. *J. Computat. Chem.* **16**:1357-1377.

Edman, K., Royant, A., Nollert, P., Maxwell, C.A., Pebay-Peyroula, E., Navarro, J., Neutze, R., Landau, E.M., 2002 Early Structural Rearrengements in the Photocycle of an Integral Membrane Sensory Receptor. *Structure*, **10**:473-482

Frisch, M. J., Trucks, G. W., Schlegel, H. B.; Scuseria, G. E.; Robb, M. A., Cheeseman, J. R., Zakrzewski, V. G., Montgomery, J. A. Jr., Stratmann, R. E., Burant J. C., Dapprich, S., Millam, J. M., Daniels, A. D., Kudin, K. N., Strain, M. C., Farkas, O., Tomasi, J., Barone, V., Cossi, M., Cammi, R., Mennucci, B., Pomelli, C., Adamo, C., Clifford, S., Ochterski, J., Petersson, G. A., Ayala, P. Y., Cui, P., Morokuma, K., Malick, D. K., Rabuck, A. D., Raghavachari, K., Foresman, J. B., Cioslowski, J., Ortiz, J. V., Baboul, A. G., Stefanov, B. B., Liu, G., Liashenko, A., Piskorz, P., Komaromi, I., Gomperts, R., Martin, R. L., Fox, D. J., Keith, T., Al-Laham, M. A.,Peng, C. Y., Nanayakkara, A., Gonzalez, C., Challacombe, M., Gill, P. M. W., Johnson, B., WChen, Wong, M. W., Andres, J. L., Gonzalez, C., Head-Gordon, M., Replogle, E. S., and Pople J. A., *Gaussian 98,Revision A.7*, Gaussian, Inc., Pittsburgh PA, 1998.

Furutani, Y., Iwamoto, M., Shimono, K., Kamo, N., and Kandori, H., 2002 FTIR Spectroscopy of the M photointermediate in *pharaonis* Phoborhodopsin. *Biophysical Journal* **83**:3482-3489

Gordeliy, V.I., Labahn, J., Moukhametzianov, R., Efremov, R., Granzin, J., Schiesinger, R., Buldt, G., Savopol, T., Scheidig,A.J., Klare, J.P., & Engelhard, M., 2002 Molecular basis of transmembrane signaling by sensory rhodopsin II - transducer complex. *Nature* **419**:484-487.

Hippler-Mreyen, S., Klare, J.P., Wegener, A.A., Seidel, R., Herrmann, C., Schmies, G., Nagel, G., Bamberg, E., Engelhard, M. 2003. Probing the Sensory Rhodopsin II Binding Domain of its Cognate Transducer by Calorimetry and Electrophysiology. *J. Mol. Biol.* **330**:1203-1213.

Humphrey, W., Dalke, A. and Schulten, K. 1996. VMD - Visual Molecular Dynamics, *J. Molec. Graphics*, **14**:33-38.

Joshi, M.K., Dracheva, S., Mukhopadhyay, A.K., Bose, S. & Hendler, R.W. 1998 Importance of Specific Native Lipids in Controlling the Photocycle of Bacteriorhodopsin. *Biochemistry* **37**:14463-14470.

Kamo, K., Shimono, K., Iwamoto, M., and Sudo, Y. 2001. Photochemistry and Photoinduced Proton-Transfer by Pharaonis Phoborhodopsin. *Biochemistry* **66**:1580-1587

Kandori, H., Shimono, K., Sudo, Y., Iwamoto, M., Shichida, Y. and Kamo, N. 2001. Structural Changes of *pharaonis* Phoborhodopsin upon Photoisomerization of the Retinal Chromophore: Infrared Spectral Comparison with Bacteriorhodopsin. *Biochemistry* **40**:9238-9246.

Kates, M., Moldoveanu, N. & Stewart, L.C., 1993 On the revised structure of the major phospholipid of Halobacterium salinarium. *Biochimica et Biophysica Acta* **1169**:46-53.

Klare, J.P., Gordeliy, V.I., Labahn, J., Buldt, G., Steinhoff, H.-J., Engelhard, M. 2004. The archaeal sensory rhodopsin II/transducer complex : a model for transmembrane signal transfer. *FEBS Letters* **569**:219-224

Koch, M.H., Dencher, N.A., Oesterhelt, D., Plohn, H.J., Rapp, G., and Buldt, G. 1991. Time-resolved X-ray diffraction study of structural changes associated with the photocycle of bacteriorhodopsin. *EMBO J.* **10**: 521-526.

Kollmann, P.A., Massova, I., Reyes, C., Kuhn, B., Huo, S., Chong, L., Lee, M., Lee, T., Duan, Y., Wang, W., Donini, O., Cieplak, P., Srinivasan, J., Case, D.A. & Cheatham,III T.E., 2000 Calculating Structures and Free Energies of Complex Molecules: Combining Molecular Mechanics and Continuum. *Models. Accts. Chem. Res.* **33**:889-897

Lee, Y.-S., 2004 Dynamics of Proton Transfer in Bacteriorhodopsin *J. Am. Chem. Soc.* **126**:2225-2230.

Lee, C., Yang, W. and Parr, R.G., 1988 Development of the Colle-Salvetti correlation-energy formula into a functional of the electron density. *Phys. Rev. B* **37**:785-789.

Mitsuoka, K., Hirai, T., Murata, K., Miyazawa, A., Kidera, a., Kimura, Y. and Fujiyoshi Y., 1999 The Structure of Bacteriorhodopsin at 3.0A Resolution Based on Electron Crystallography:Implication of the Charge Distribution *J. Mol. Biol.* **286**:861-882.

Murata, K., Fujii, Y., Enomoto, N., Hata, M., Hoshino, T., Tsuda, M. 2000. A study on the mechanism of the proton transport in bacteriorhodopsin : The importance of the water molecule, *Biophys. J.* **79**: 982-991

Murata, K., Hoshino, T., Sato, Y., Hata, M. and Tsuda, M., 2003 Unidirectional proton transfer mechanism in the L-M-N sequence of Bacteriorhodopsin, *J. Mol. Struct.: THEOCHEM*, **664/665:**125-133

Murata, K., Hoshino, T., Sato, Y., Hata, M., Tsuda, M., 2002 A factor to determine the direction of the proton transfer in bacteriorhodopsin, *Chem-Bio Inform. J.* **2**:97-103

Royant, A., Nollert , A., Edman, K., Neutze, R., Landau, E.M., Pebay-Peyroula, E., Navarro, J. 2001. X-ray structure of sensory rhodopsin II at 2.1-angstrom resolution. *Proc. Natl. Acad. Sci. U.S.A.* **98**:10131-10136.

Sasaki, J. & Spudich, J.L. 1999. Proton circulation during the photocycle of sensory rhodopsin II. *Biophysical J.* **77**:2145-2152

Sayle, R. and Milner-White, E.J., 1995. RasMol: Biomolecular graphics for all, *Trends in Biochemical Sciences (TIBS)*, **20**: 9-374.

Schobert, B., Brown, L.S. and Lanyi, J.K., 2003 Crystallographic Structures of the M and N Intermediates of Bacteriorhodopsin: Assembly of a Hydrogen-bonded Chain of Water Molecules Between Asp-96 and the Retinal Schiff Base, *J. Mol. Biol.* **330**:553-570.

Seidai, R., Scharf, B., Gautel, M., Kleine, K., Oesterhelt, D., Engelhard, M. 1995. The primary structure of sensory rhodopsin II: a member of an additional retinal protein subgroup is coexpressed with its transducer, the halobacterial transducer of rhodopsin II. *Proc. Natl. Acad. Sci. U.S.A.* **92**:3036-3040.

Spudich, E.N., Zhang, W., Alam, M., Spudich, J.L. 1997 Constitutive signaling by the phototaxis receptor sensory rhodopsin II from disruption of its protonated Schiff base - Asp73 interhelical salt bridge. *Proc. Natl. Acad. Sci. USA* **94**:4960-4965.

Subramaniam, S., Gerstein, M., Oesterhelt, D. & Henderson, R. 1993 Electron diffraction analysis of□@structural changes in the photocycle of bacteriorhodopsin. *EMBO J.* **12**:1-8.

Sudo, Y., Yamabi, M., Iwamoto, M., Shimono, K. and Kamo, N. 2003. Interaction of Natronobacterium pharaonis Phoborhodopsin (Sensory Rhodopsin II) with its Cognate Transducer Probed by Increase in the Thermal Stability. *Photochemistry and Photobiology* **78**:511-516.

Tajkhorshid, E., Baudry, J., Schulten, K. & Suhai, S. 2000. Molecular Dynamics Study of the Nature and Origin of Retinal's Twisted Structure in Bacteriorhodopsin. *Biophysical J.* **78**:683-693.

Takahashi, T., Yan, B., Mazur, B., Derguini, F., Nakanishi, K. & Spudich, J.L. 1990. Color Regulation in the Archaebacterial Phototaxis Receptor Phoborhodopsin (Sensory Rhodopsin II). *Biochemistry*, **29**:8467.

Takahashi, T., Tomioka, H., Kamo, N. and Kobatake, Y. 1985. A photosystem other than PS370 also mediates the negative phototaxis of Halobacterium halobium. *FEMS Microbiol. Letters.* **28**:161-164.

Thompson, J.D., Higgins, D.G., Gibson, T.J. 1994. CLUSTAL W: improving the sensitivity of progressive multiple sequence alignment through sequence weighting, position-specific gap penalties and weight matrix choice. *Nucleic Acids Res.* **22**:4673-4680

Wang , J., Cieplak, P. & Kollmann, P.A. 2000. How well does a restrained electrostatic potential (RESP) model perform in calculating conformational energies of organic and biological molecules? *J. Comput. Chem*. **21**:1049-1074.

Wegener, A. A., Klare, J.P., Engelhard, M. & Steinhoff, H. J. 2001. Structural insights into the early steps of receptor-transducer signal transfer in archaeal phototaxis. *EMBO J.* **20**:5312-5319.

Wegener, A.A., Chizhov, I., Engelhard, M. & Steinhoff, H.J. 2000. Time-resolved detection of transient movement of helix F in spin-labelled pharaonis sensory rhodopsin II. *J. Mol. Biol.* **301**:881-891.

Zhang, X.N., Zhu, J. & Spudich, J. L., 1999. The specificity of interaction of archaeal transducers with their cognate sensory rhodopsins is determined by their transmembrane helices. *Proc. Natl. Acad. Sci. USA*, **96:**857-862

Table Title

Table 1

Hydrogen bonds between helixF and other helices of sRII.

Table2

Hydrogen bond between HtrII and sRII in the ground state.

Table3

Affinity changes calculated with MM_GBSA method.

[Figure Captions]

Fig1

Simulation model for sRII – HtrII – lipid layer– solvent water system

(a) sRII – HtrII complex inserted into the cavity of lipid bilayer manually (b) Structure of a component of the lipid bilayer:PGP-ME (phosphatidylglycerophosphate monometyl ester). PGP-Me is the main component of purple membrane (PM)(c) The model containing the water molecules at the upper and lower sides of the lipid – protein complex (d) The lipid – protein complex viewed from the cytoplasmic side

Waters are not shown for the sake of visual clarity

Fig2

The fluctuation of the thickness of lipid bilayer (the average distance between the hydroxyl group's oxygen atoms of glycerol) during the equilibrating and the subsequent dynamics simulations in the ground state. Dash line shows that the value of the thickness obtained by the electron diffraction experiment in *Halobacterium salinarium* (Mitsuoka et al., 1999).

Fig3

Distance between Schiff base and two amino acid residues as a function of simulation time in three intermediates.

(a) The distance between Schiff base and oxygen atom of hydroxyl side chain of Thr79. (b) The distance between Schiff base and oxygen atom of calboxyl side chain of Asp201.

Fig4

Sketch of the hydrogen bond network between helixF and other helices of sRII viewed from the cytoplasmic side. The thick arrow is the direction of the movement of helixF proposed by EPR experiments (Wegener et al., 2000).

Fig5

Distance between the center of sRII (residue 1-225) and the center of cytoplasmic half side (residue 158-170) in the course of the simulation.

Fig6

Superimposed structure of M-state and the ground state. Each structure is the average of the last 50ps of the simulation. A green ball represents the center of whole protein, and red and blue balls represent the center of the cytoplasmic side (res 158 -170) of helixF. Arrow shows the direction of movement of helixF in M-state.

Fig.7

(a)Van der Waals interaction energy between retinal and each residue of sRII.

(b) Degree of sequence conservation among 16 bacterial retinal-proteins (bR,hR,sRI,sRII).

First, we aligned the amino acid sequence of the 16 retinal proteins, then determined the degree of amino acid sequence conservation of *Natronobacterium pharaonis* sRII. The degree is calculated from the following equation; degree = (the number of proteins in which sRII sequence is conserved at the corresponding position)/ (total number of bacterial retinal proteins)

(c) Difference of van der Waals interaction energy between M-state and the ground state. The negative value means that the interaction becomes week in M-state than the ground state.

Fig.8

Superimposition of atom geometry between M-state and K-state. Each geometry was obtained from the average structure during the last 50ps of the MD simulation. M-state is represented by ball and stick. And K-state structure is represented by thin stick.

Fig.9

(a)Conformational changes of cytoplasmic side of TM2 in the course of 2ns MD simulation, viewed from the cytoplasmic side. Each structure was superimposed to the initial structure of M-state MD simulation. Red balls represent C_α carbon atoms of the three amino acid residues (Ala79,Ala80,Thr81) of TM2 in the initial structure. Blue balls represent those in the snap shot structure at each simulation time. Rotational angle of each amino acid residue from the initial structure is shown below the snap shot structure at the respective simulation time.

(b)Side chain locations of these three amino acid residues. The initial structure is represented by sticks and the snapshot structure at 1800ps by ball and stick. (1)~(3) show the displacement of methyl carbon atoms in the 1800ps snapshot structure measured from the initial structure. Black arrow represents the direction of each amino acid residue's movement, and red arrow represents the rotational direction of TM2.

Fig10

(a)Van der Waals(VDW) and Coulomb(EEL) interaction energy between HtrII and each amino acid residues of helixF and helixG (sRII). The residues marked with circle had the large interaction with HtrII.

(b)Van der Waals(VDW) and Coulomb(EEL) and solvation(SOL) interaction energy between HtrII and each amino acid residues of helixF and helixG (sRII)

Table1

Donor		Acceptor	Average distance (Å)	Occupied (%)	Partner Helix
Tyr160 –OH	HH	*Leu141 –O	2.907	99.8	E
*Arg164 – NH2	HH21	*Leu141 – O	3.713	80.8	E
*Arg164 – NH2	HH21	Val142 – O	3.480	73.2	E
*Arg164 – NH2	HH21	*Thr146 -OG1	2.927	100	E
*Arg164 – NE	HE	*Leu141- O	2.982	100	E
*Arg164 – NE	HE	*Thr146 – OG1	3.848	52.4	E
*Tyr174 – OH	HH	*Asp201–OD1	2.734	100	G
*Trp178 – NE1	HE1	*Tyr73 – OH	3.531	60.6	C
*Trp178 – NE1	HE1	Gly112 – O	3.414	97.0	D
*Arg123 – NH2	HH21	Pro183 – O	3.738	48	E
*Arg123 – NE	HE	Pro183 – O	2.886	100	E
*Thr204 – OG1	HG1	*Tyr174 – OH	2.965	99.8	D

Asterisk means that the amino acid residue is conserved at the corresponding sequence of BR. Average distance is of between donor and acceptor atoms. Occupied(%) means the percentage in time for clearing the hydrogen bond criteria during the ground state simulation. Partner helix means the counterpart connecting with helixF through the hydrogen bond.

Table2

Donor		acceptor	Average distance (Å)	Occupied (%)	BR_res
*Tyr199(G)-OH	HH	Phe28-O	3.03	91.417	Val
*Tyr199(G)-OH	HH	Thr33-OG1	3.256	98.403	Val
*Arg162(F)-NE	HE	Ala80-O	3.229	86.626	Val
*Thr189(G)-OG1	HG1	Glu43-OE2	2.882	100	Pro
*Thr189(G)-N	H	Ser62-OG	3.002	100	Pro
*Thr191(G)-OG1	HG1	Glu43-OE1	2.866	100	(Asn)
*Thr191(G)-OG1	HG1	Glu43-OE2	3.660	89.82	(Asn)
Asn74-ND2	HD21	*Tyr199(F)-OH	3.178	58.88	Val

Asterisk indicates that the residue belongs to HtrII.

BR_res shows the amino acid residue corresponding in BR.

Table3

Mutation	**ΔΔG**	**Helix**
wild	0	F
S150E	0.04	F
Q151S	-0.14	F
R152M	0.09	F
K157A	0.31	F
R162V	3.99	F
T189P	10.84	G
T191N	-2.24	G
V198M	-0.265	G
Y199M	10.82	G

ΔΔG = ΔG_mutation – ΔG_wildtype

ΔG = ΔG(VDW) + ΔG(Coulomb) + ΔG(solvation)

The positive value of ΔΔG means that the affinity decreases due to the mutation. Three mutations (R162V, T189V, Y199V) have large influences on the binding affinity.

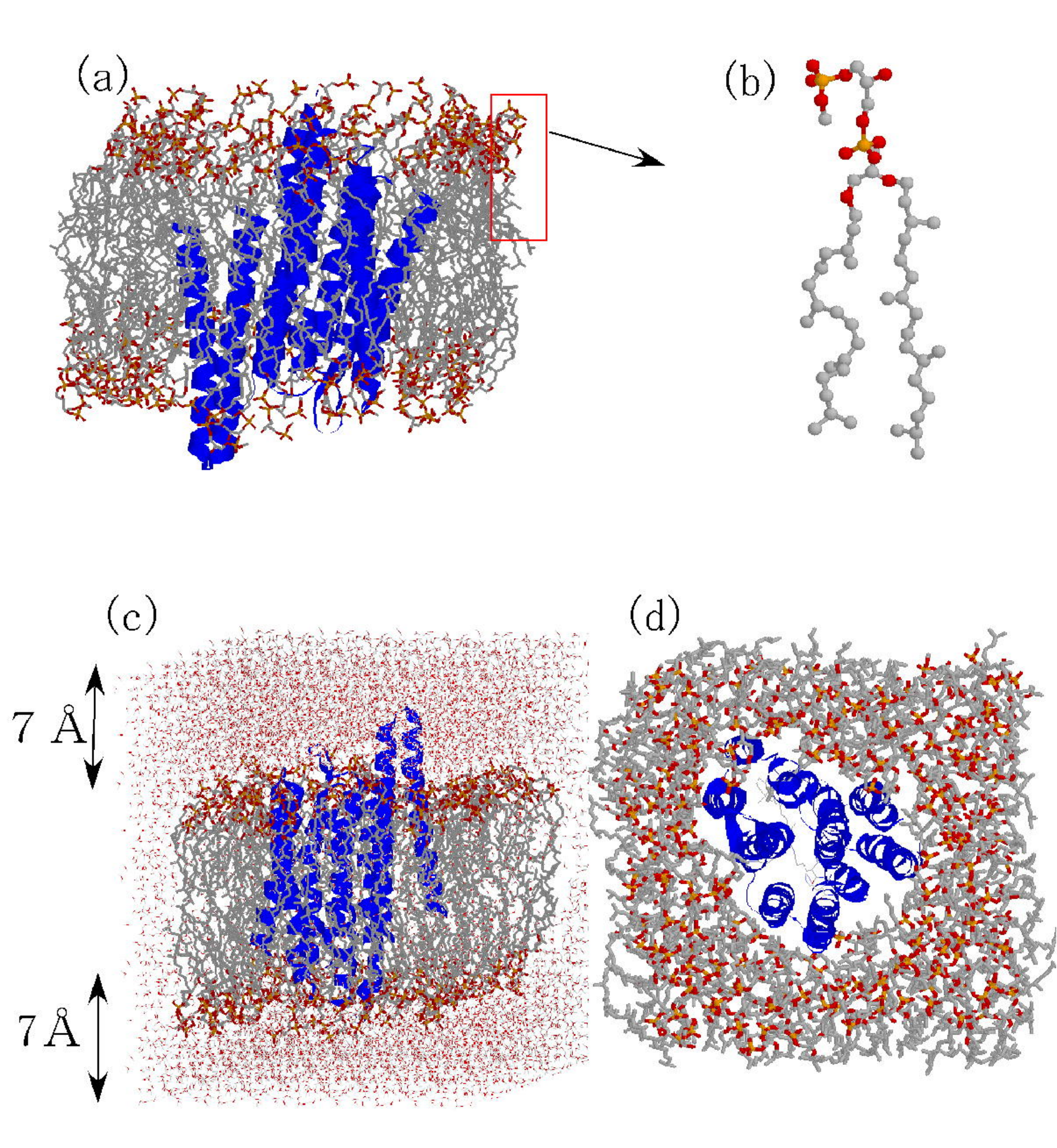
(a)
(b)
(c)
(d)
7 Å
7 Å

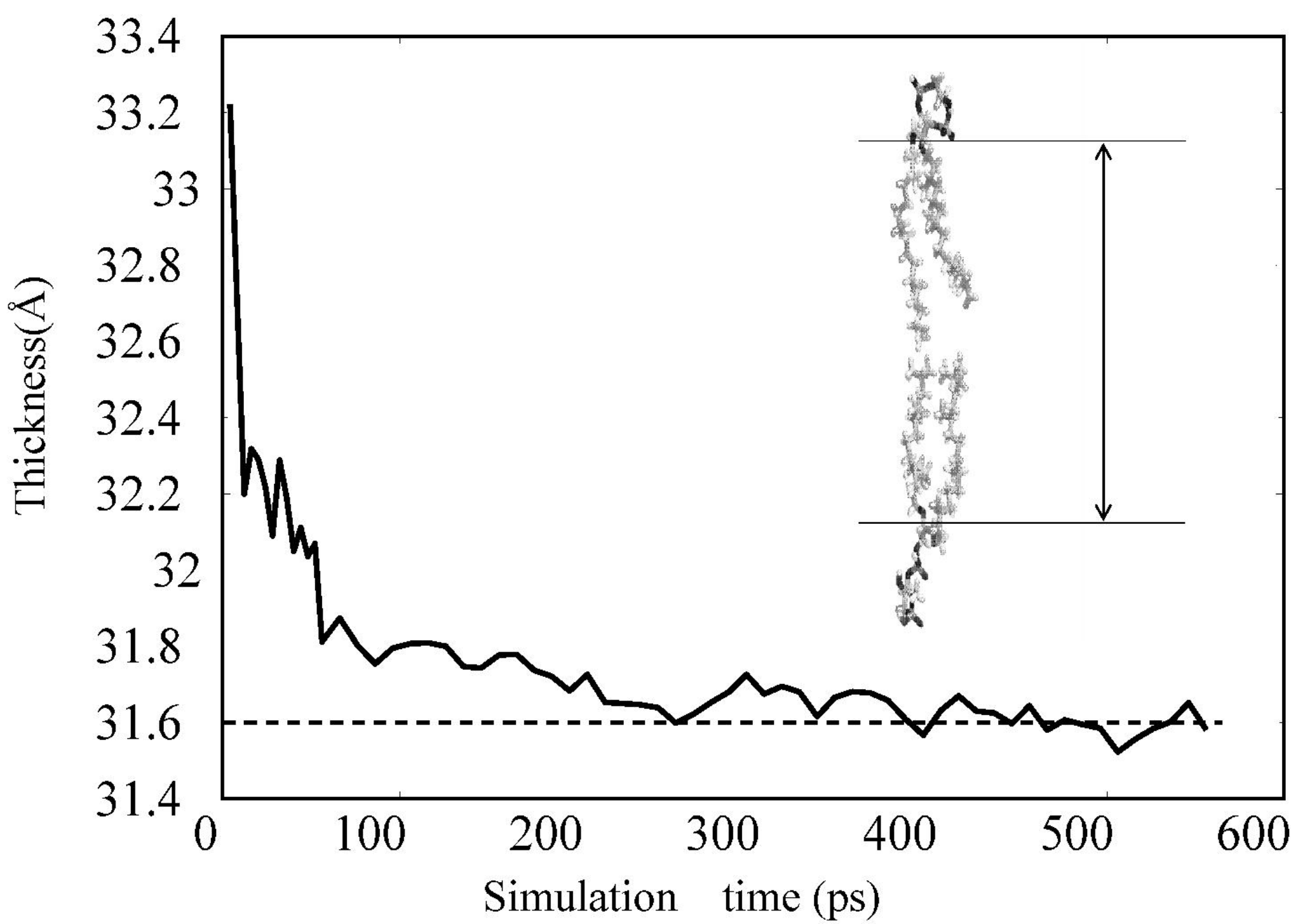
33.4
33.2
33
32.8
32.6
32.4
32.2
32
31.8
31.6
31.4
Thickness(Å)
0
100
200
300
400
500
600
Simulation time (ps)

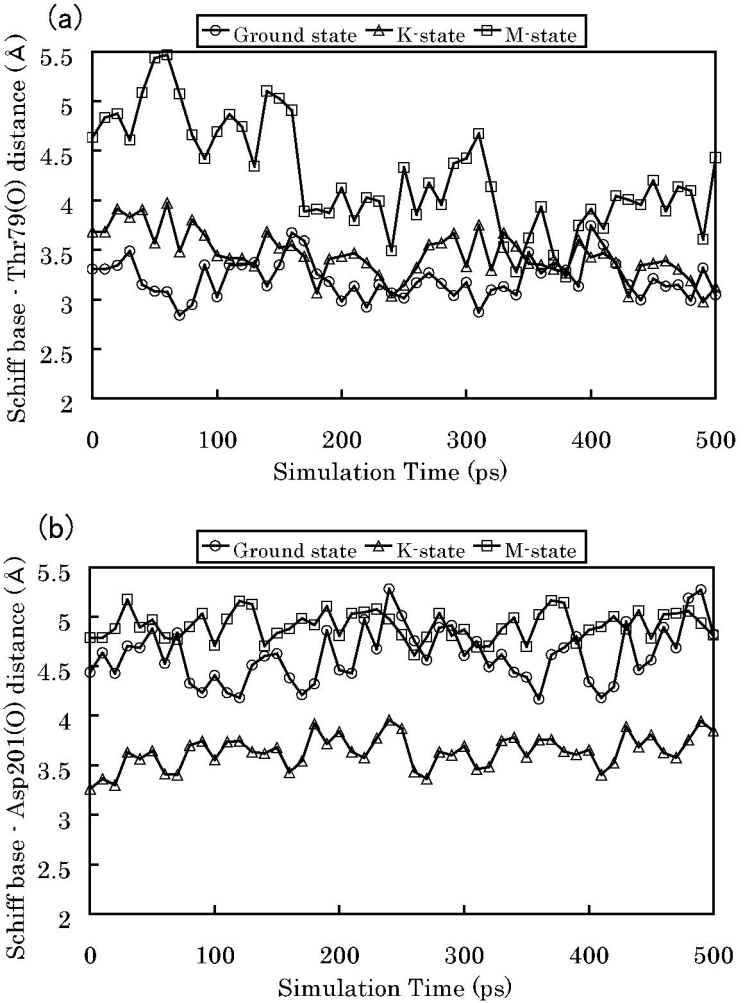
(a)
Ground state
K-state
M-state
Schiff base - Thr79(O) distance (Å)
5.5
5
4.5
4
3.5
3
2.5
2
0
100
200
300
400
500
Simulation Time (ps)
(b)
Ground state
K-state
M-state
Schiff base - Asp201(O) distance (Å)
5.5
5
4.5
4
3.5
3
2.5
2
0
100
200
300
400
500
Simulation Time (ps)

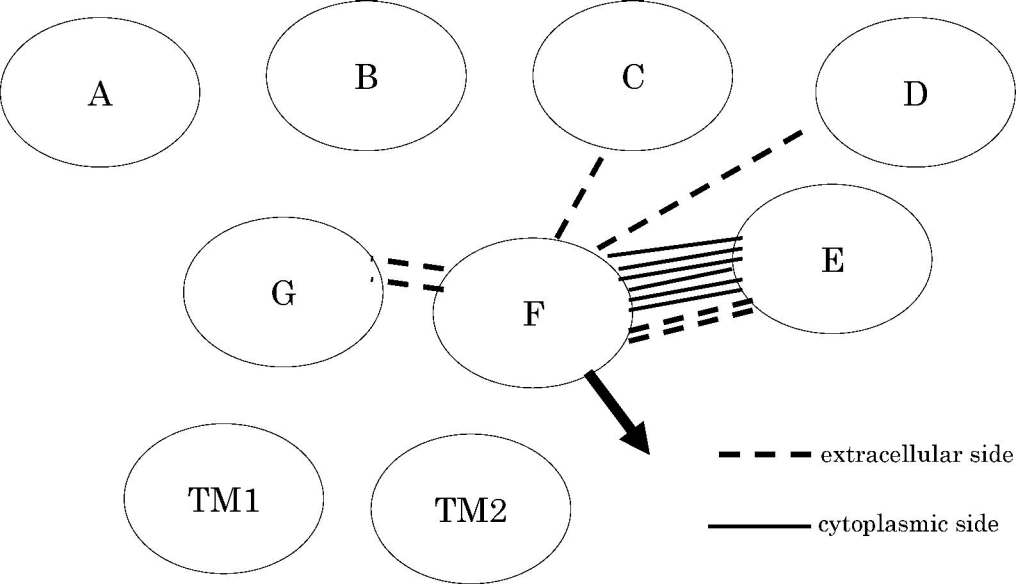
A
B
C
D
E
F
G
TM1
TM2
extracellular side
cytoplasmic side

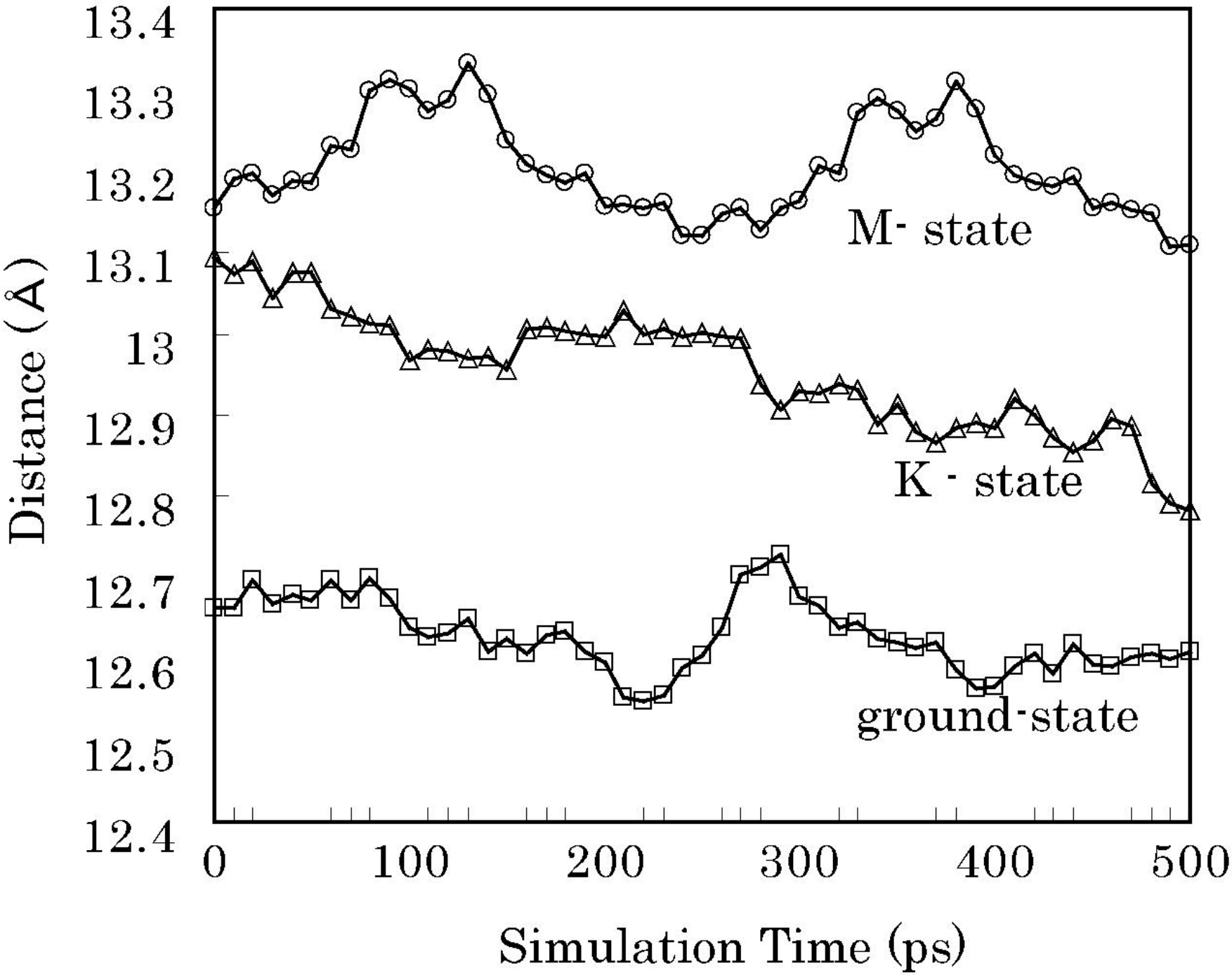
13.4
13.3
13.2
13.1
13
12.9
12.8
12.7
12.6
12.5
12.4
Distance (Å)
M- state
K - state
ground-state
0
100
200
300
400
500
Simulation Time (ps)

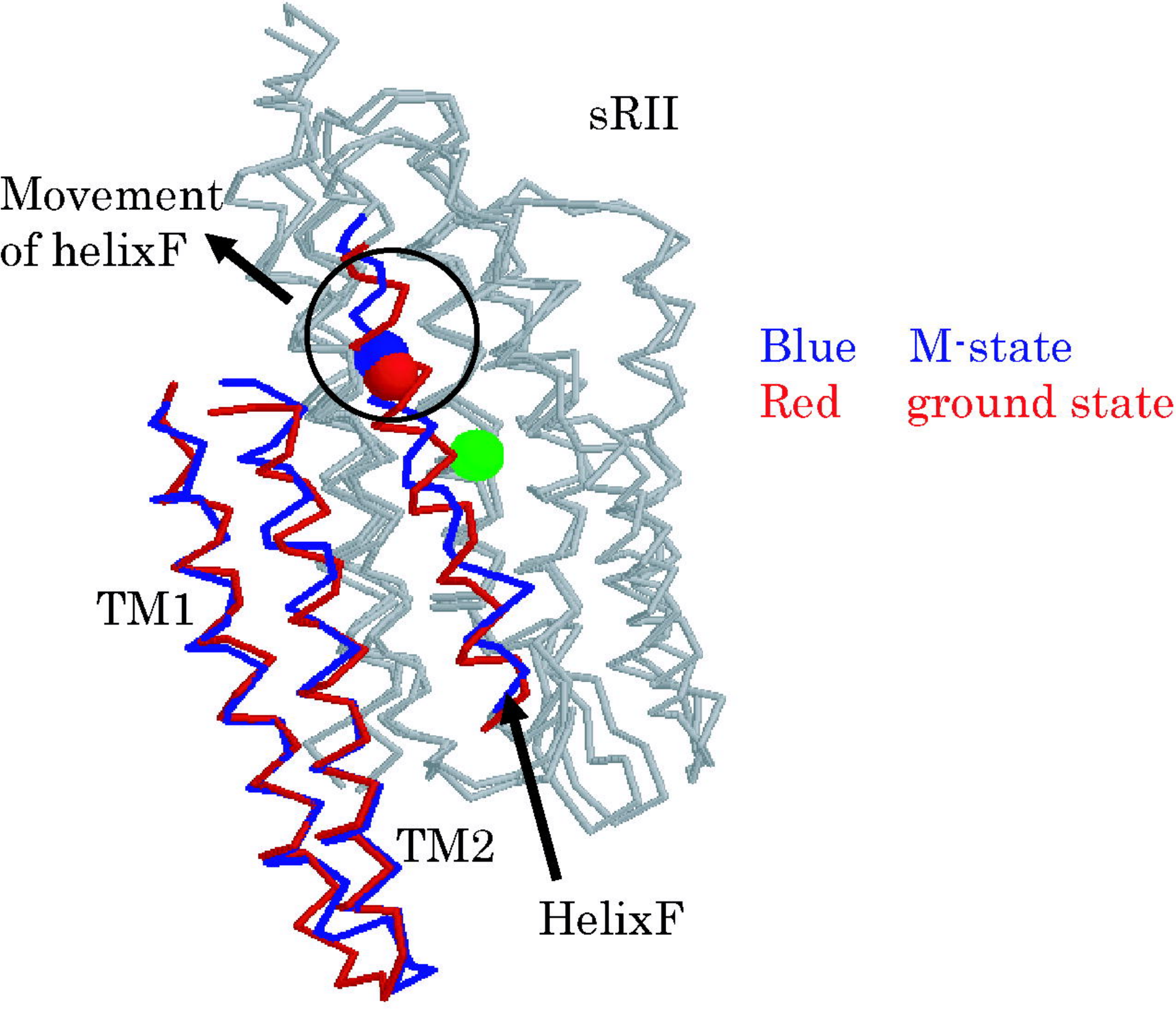
sRII
Movement
of helixF
TM1
TM2
HelixF
Blue M-state
Red ground state

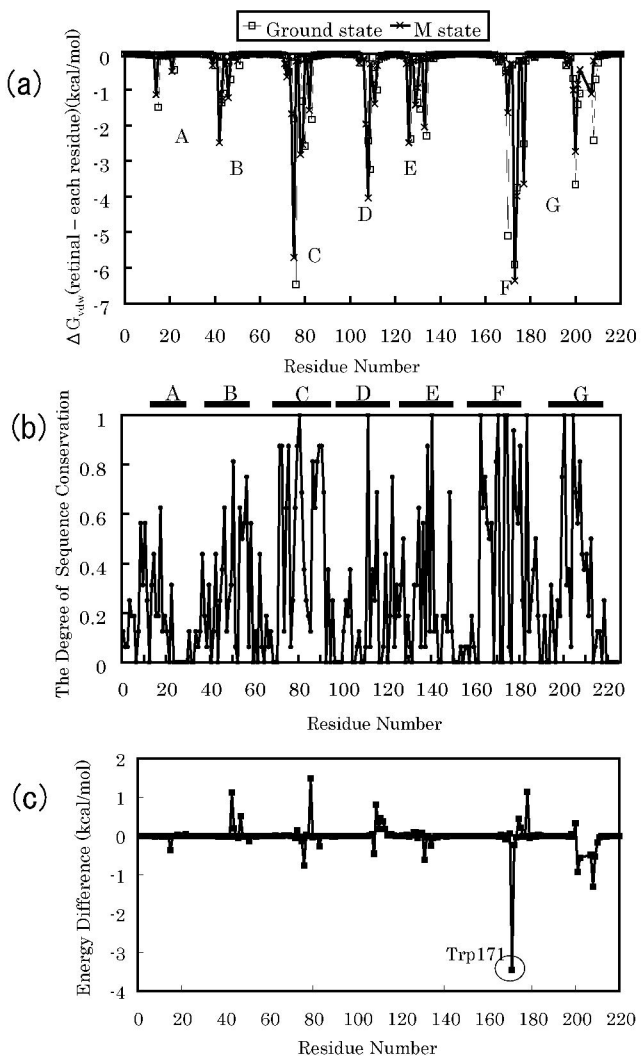
(a)
Ground state
M state
ΔG_{vdw} (retinal – each residue) (kcal/mol)
A
B
C
D
E
F
G
Residue Number
(b)
The Degree of Sequence Conservation
Residue Number
(c)
Energy Difference (kcal/mol)
Trp171
Residue Number

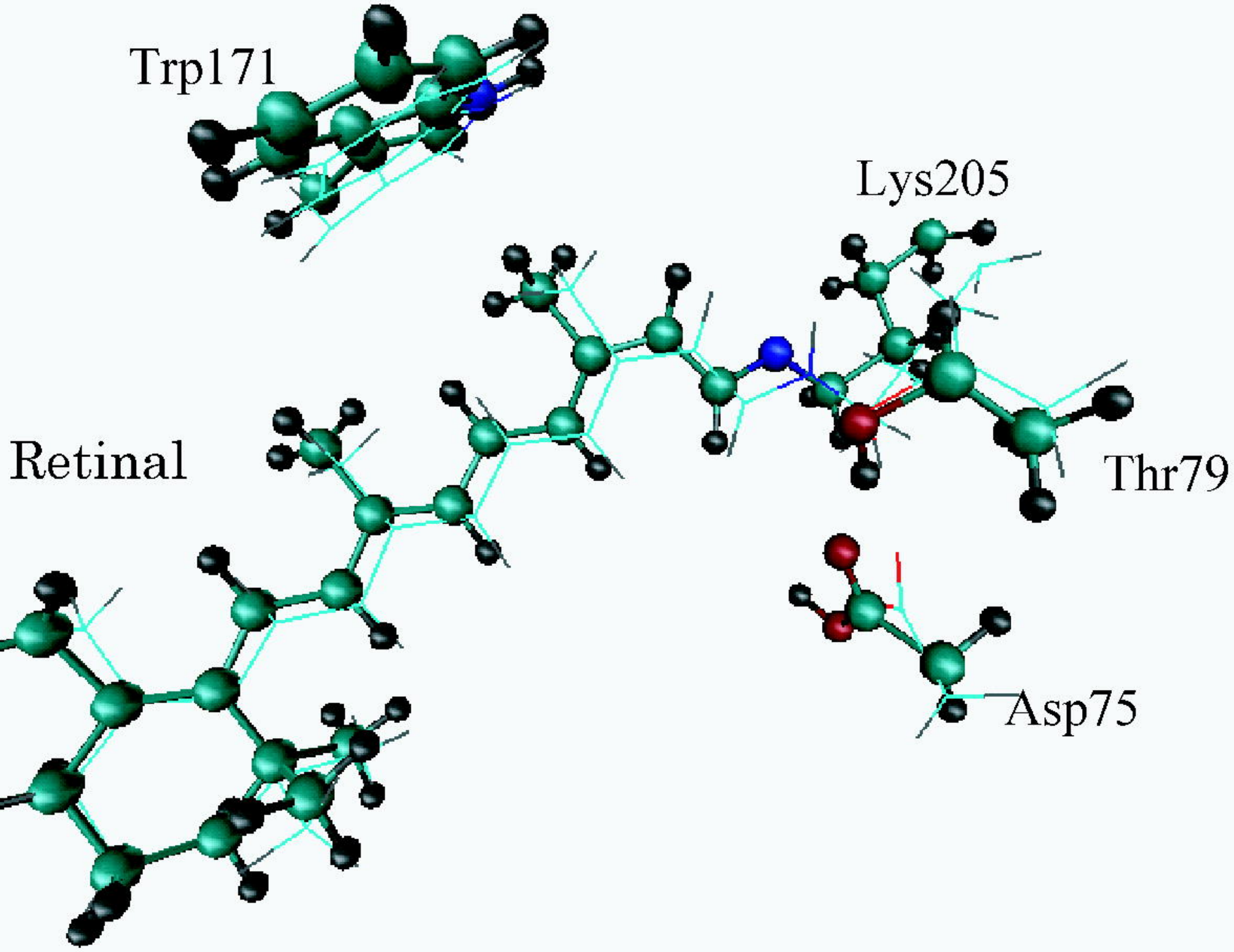
Trp171
Lys205
Retinal
Thr79
Asp75

(a)

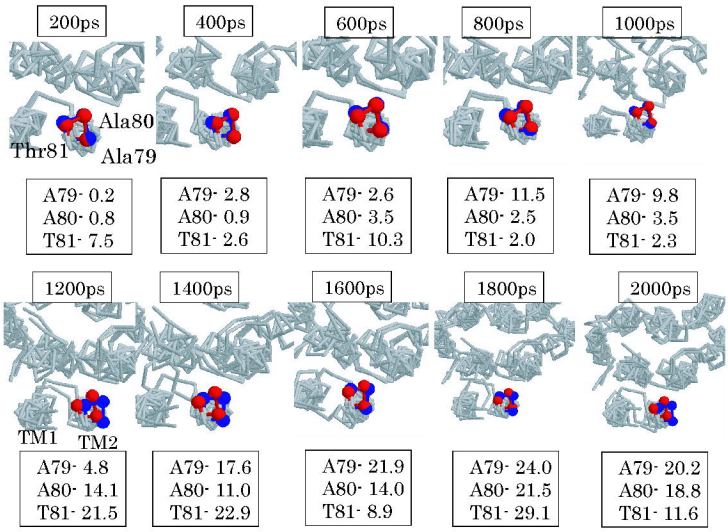
200ps
400ps
600ps
800ps
1000ps
Ala80
Thr81
Ala79
A79- 0.2
A80- 0.8
T81- 7.5
A79- 2.8
A80- 0.9
T81- 2.6
A79- 2.6
A80- 3.5
T81- 10.3
A79- 11.5
A80- 2.5
T81- 2.0
A79- 9.8
A80- 3.5
T81- 2.3
1200ps
1400ps
1600ps
1800ps
2000ps
TM1
TM2
A79- 4.8
A80- 14.1
T81- 21.5
A79- 17.6
A80- 11.0
T81- 22.9
A79- 21.9
A80- 14.0
T81- 8.9
A79- 24.0
A80- 21.5
T81- 29.1
A79- 20.2
A80- 18.8
T81- 11.6

(b)

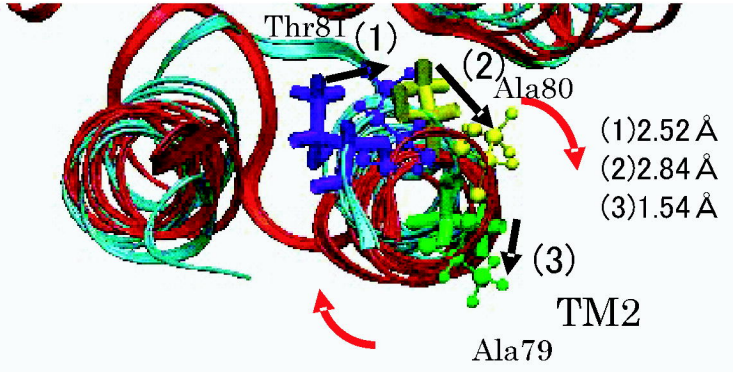
Thr81
(1)
(2)
Ala80
(1)2.52 Å
(2)2.84 Å
(3)1.54 Å
(3)
TM2
Ala79

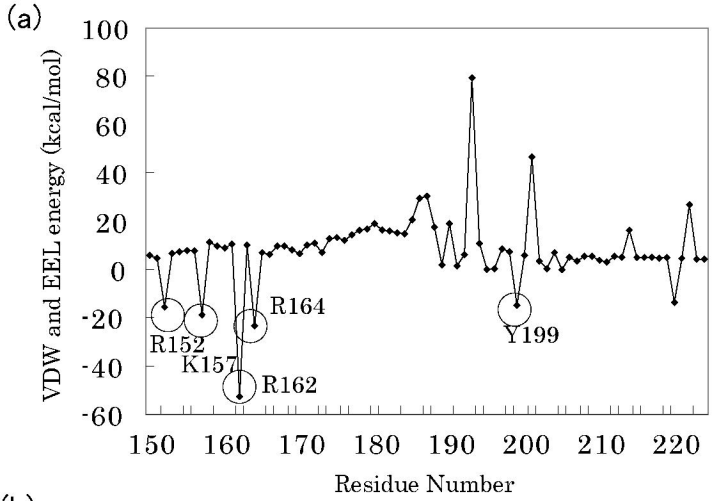
(a)
VDW and EEL energy (kcal/mol)
100
80
60
40
20
0
-20
-40
-60
R152
K157
R162
R164
Y199
150
160
170
180
190
200
210
220
Residue Number

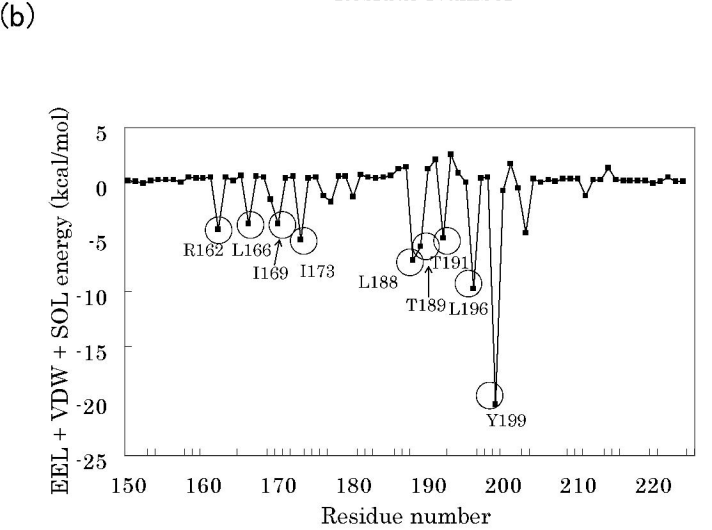
(b)
EEL + VDW + SOL energy (kcal/mol)
5
0
-5
-10
-15
-20
-25
R162
L166
I169
I173
L188
T189
I191
L196
Y199
150
160
170
180
190
200
210
220
Residue number